Model calibration and validation for pre-production EUVL

Gian F. Lorusso[*a], Jeroen Van de Kerkhove[a], Peter De Bisschop[a], Eric Hendrickx[a],
J. Jiang[b], D. Rio[b], W. Liu[b], H. Liu[b]
[a]Imec, Kapeldreef 75, 3001 Leuven, Belgium;
[b]ASML Brion, 4211 Burton Dr., Santa Clara, USA

ABSTRACT

As Extreme Ultraviolet Lithography (EUVL) enters the pre-production phase, the need to qualify the Electronic Design Automation (EDA) infrastructure is pressing. In fact, it is clear that EUV will require optical proximity correction (OPC), having its introduction shifted to more advanced technology nodes. The introduction of off-axis illumination will enlarge the optical proximity effects, and EUV-specific effects such as flare and shadowing have to be fully integrated in the correction flow and tested.

We have performed a model calibration exercise on the ASML NXE:3100 pre-production EUVL scanner using Brion's Tachyon NXE EUV system. A model calibration mask has been designed, manufactured and characterized. The mask has different flare levels, as well as model calibration structures through CDs and pitch. The flare modulation through the mask is obtained by varying tiling densities. The generation of full-chip flare maps has been qualified against experimental results. The model was set up and calibrated on an intermediate flare level, and validated in the full flare range.

Wafer data have been collected and were used as input for model calibration and validation. Two-dimensional structures through CD and pitch were used for model calibration and verification. We discuss in detail the EUV model, and analyze its various components, with particular emphasis to EUV-specific phenomena such as flare and shadowing.

Keywords: EUVL, EUV, OPC, Flare, Shadowing, Resist Model, NXE:3100

1. INTRODUCTION

The Extreme Ultraviolet Lithography (EUVL) scanner prototypes have been operational in the field for a few years now, providing crucial information on the potential of EUVL by demonstrating the feasibility of 32nm and 22nm node devices [1,2], the relatively marginal impact of optics contamination, and the predictability of EUV-specific effects such as shadowing and flare [3,4]. These results strengthened the confidence in EUVL, and the alpha tools are now being replaced with pre-production tools delivering higher throughput and better performances. However, as the introduction of EUVL in production has shifted to more advanced nodes, the accuracy of optical proximity correction (OPC) and the effectiveness of the Electronic Design Automation (EDA) infrastructure are critical to its success in handling larger σ settings and off-axis illumination [5]. EUV-specific effects need to be properly qualified and fully integrated in the correction flow in order to meet the tight CDU specifications, and OPC is imperative to ensure pattern fidelity for advanced technology nodes.

In this study, a model calibration exercise on the pre-production EUVL scanner is performed for contact holes (CH), likely to be the most used layer in EUVL. A dedicated model calibration mask having multiple flare levels, calibration structures through critical dimension (CD) and pitch, as well as repeats through slits and scans has been designed, manufactured and characterized. The good quality of the model calibration mask is a critical factor. The flare modulation is obtained by local variations of the tiling density, and the accuracy of simulated full-chip flare maps has been tested against experimental results. Wafer data have been collected and used as input for model calibration and validation. The model was calibrated using intermediate flare levels and validated in the full flare range and across slit. A variety of two-

[*] lorusso@imec.be

Extreme Ultraviolet (EUV) Lithography III, edited by Patrick P. Naulleau,
Obert R. Wood II, Proc. of SPIE Vol. 8322, 83221L · © 2012 SPIE
CCC code: 0277-786X/12/$18 · doi: 10.1117/12.916762

dimensional structures through CD and pitch were used for model calibration and verification. The characteristics of the calibrated EUV model, with particular emphasis to EUV-specific effects are discussed.

2. MODEL CALIBRATION AND VERIFICATION MASK

The mask layout used for model calibration and verification in this study is reported in Figure 1, where its flare map is shown. The flare variation is achieved by modulating the tiling density across the mask. The layout has five repetitions through scan at different flare levels, as well as seven repeats through slit at the same flare level. The position (x, y) of each module is defined relatively to the central module (0, 0). For example, the module in the top left corner will be (-3, 2).

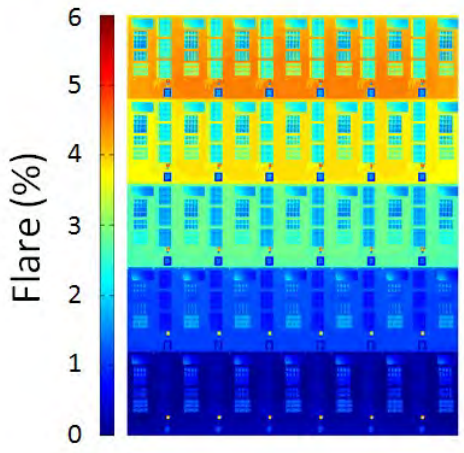

Figure 1: Flare map generated for the layout used in this study. Inter field effects and exit aperture effects were considered during flare map generation.

Each individual module has four 2D sub-modules, containing CH through pitch (sub-module CH 1), CH with asymmetric pitch in x and y (sub-module CH 2), elongated CH with different CD in x and y (sub-module CH 3), and various types of CH arrangements (sub-module CH4), as illustrated in Figure 2.

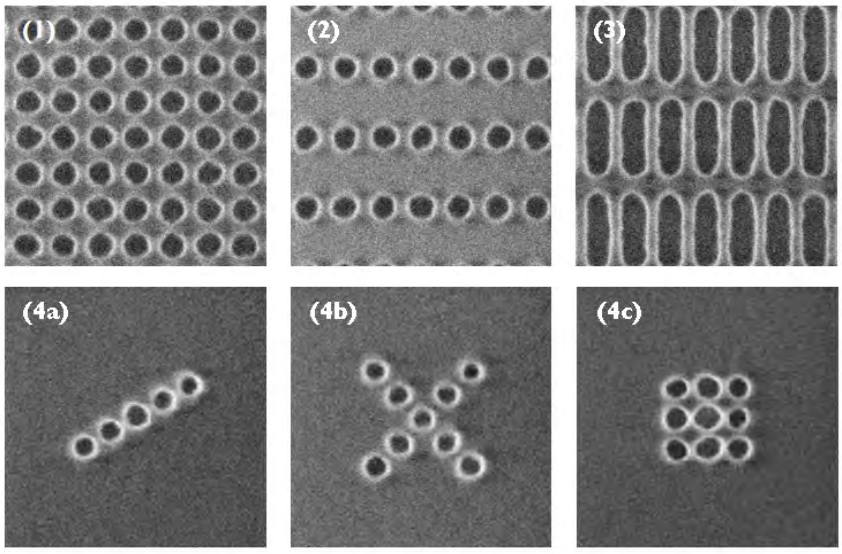

Figure 2: Example of structures in the four 2D sub-modules: (1) CH through pitch; (2) CH with asymmetric pitch in x and y; (3) CH with asymmetric CD in x and y; (4a-c) CH in various arrangements.

Two rounds of metrology consisting of 384 and 958 measurements were performed to qualify the mask structures. All 2D features have been measured along both x and y direction. During the first round of metrology, the mask critical dimension uniformity (CDU) and mean to target (MTT) across the mask were verified for a variety of structures, such as dense CH, dense and isolated spaces. The first metrology round evidenced the presence of a radial CD signature on the mask, with larger features in the center. The measured CDU for 32 nm dense CH was 1.6 nm (x) and 2.0 nm (y), while the MTT of these features was -0.62 nm (x) and -0.75 nm (y), confirming the high quality of the mask. All the mask measurements reported here are at 1× magnification.

The second metrology round focused on mask proximity and linearity by measuring CH and spaces in both orientations through pitch and CD in the center of the mask. The linearity for CH was estimated to be 1.01 (x) and 1.00 (y), respectively. The results indicated an average MTT through pitch and CD of -0.83 nm (x) and -0.91 nm (y) for CH, in agreement with the results obtained in the first round of metrology. The average MTT for spaces was estimated to be -0.95 nm (x) and -0.92 nm (y), very similar to the one of CH. In terms of mask proximity, the mask bias between isolated and dense CH was observed to have an amplitude of 1.23 nm, as shown by the behavior of the MTT through pitch in Figure 3. As in the case of the first metrology round, the results confirmed the good quality of the mask used in this exercise.

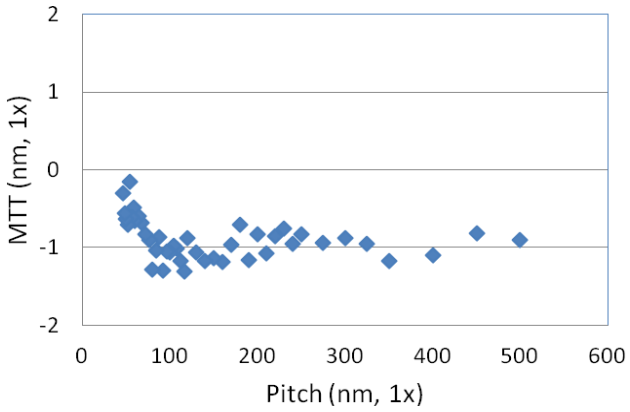

Figure 3: Mask MTT through pitch.

3. SELECTION OF STRUCTURES FOR MODEL CALIBRATION

In a model calibration exercise it is critical to use a set of test structures able to represent as closely as possible the entire modeling space. It is equally important, however, to minimize the unproductive wafer measurement time related to the analysis of redundant structures, i.e. features providing information on very similar regions in the parameter space. Selection of the contact-hole cases used for the OPC-model calibration was done in the following way. The test mask contains several thousand contact-array cases, square and rectangular contacts. Each of these corresponds to a specific x-and y-pitch and x- and y-size. For each of these cases we ran a Prolith calculation of the image-in-resist along the x and the y axis (through the contact center), from which we extracted the numerical value of five quantities (such as minimum and maximum intensity along these axes) which we call the 'image parameters'. Each pitch-size contact case can then be represented as a point in a 5-dimensional "Image-Parameter Space (IPS)". We then obtain a selection of structures to be used for OPC-model calibration by dividing this space in equally-sized (5-dimensional) sub-cells and taking one CH case only for each populated cell (a smaller or larger sampling-cell size will lead to a larger or smaller selected-structure list, respectively). This is illustrated in Figure 4 where we have projected ('compressed') the IPS on a 2-dimensional subspace, for the ease of plotting. The (black) circles represent about 5000 contact cases we started with, the (red) triangles are the selection we made from these. These potential candidate structures are then screened on a printed wafer, and cases that don't print well or that have too small of a process latitude are removed, leaving us with the final list of structures for the OPC-model calibration. This structure-sampling technique has been successfully used by us and others [6] in 193nm lithography: it ensures that the structures used in the model calibration cover the entire target-structure space, while avoiding over-sampling of certain areas. It is hereby assumed that 'similarity' or 'difference' between different pitch-size contact combinations can be represented by the image-parameters that are being used. This is the first time we have used this IPS-sampling method for an EUV OPC-model case.

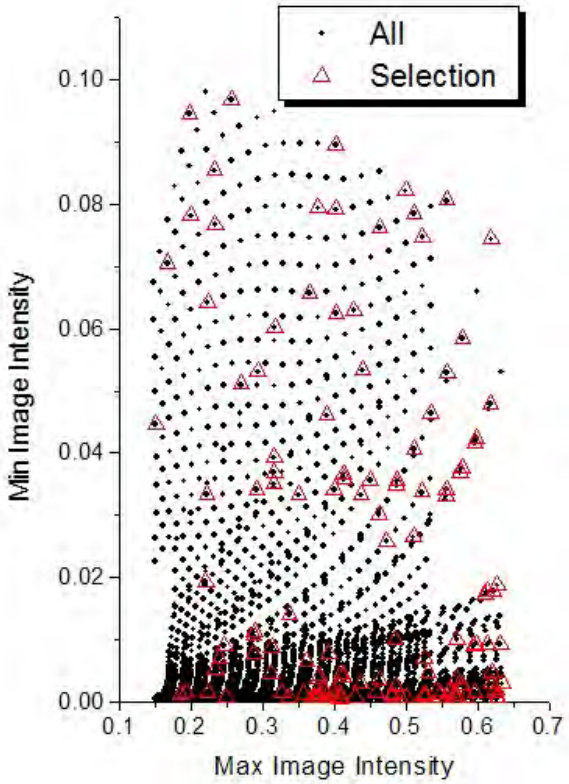

Figure 4: Illustration of the IPS-sampling method. The (black) circles represent the ~5000 contact-hole cases available on the test mask; the (red) triangles correspond to the selected sample. Note that in the original 5-dimensional IPS these selected cases are approximately equally spaced, something which is of course not apparent in the 2-dimensional compression made in this plot.

A summary of features used for model calibration and verification is reported in Table 1. The CD target for this exercise was 27 nm dense CH on wafer with a 20% mask bias. The sub-module CH 1, CH 2 and CH 3 were used for calibration, and all the calibration data have been collected in the modules (0, 0) and (2, 0). The sub-modules CH 1 and CH 4 were used for verification. The sub-module CH 1 was used for verification purpose through slit [modules (-3, 0), (-2, 0), (-1, 0), (0, 0), (1, 0), (2, 0), (3, 0)] and through scan [modules (0, 2), (0, 1), (0, 0), (0, -1), (0, -2)]. The sub-module CH 4 was used to compare the model contours to SEM images in the module (0, 0). Finally, the verification data of the proximity and correction for 27 nm CH were acquired in the module (0, 0). The total number of different features used in this exercise is 447, corresponding to 894 gauges as each feature is measured in both x and y.

Table 1 List of features in the model calibration and verification data set.

Sub-Module	Feature Type	CD	Pitch	Modeling	Feature Count
CH 1	CH through pitch	22-42 nm	44-500 nm	Calibration	42
CH 2	CH asymmetric pitch	27-47 nm	50-500 nm	Calibration	81
CH 3	Elongated CH	27-42 nm	50-500 nm	Calibration	52
CH 1	CH through pitch	22-42 nm	44-500 nm	Verification	248
CH 4	CH arrangements	27-43 nm	50-500 nm	Verification	24

4. EXPOSURES AND METROLOGY

The wafers used in this exercise have been exposed on the ASML NXE:3100 pre-production EUVL scanner using conventional illumination with NA = 0.25 and σ = 0.81. Two uniform wafers and two focus-exposure matrix (FEM) wafers were exposed for this exercise. The first wafer set was used mainly for calibration, while the second set was used for verification. The uniform wafers have been exposed at a nominal dose of 19 mJ/cm^2 and a nominal focus of 0 μm. The resist used was the Imec baseline resist, coated at a thickness of 50 nm. The FEM wafers used a nominal energy of 19 mJ/cm^2, a nominal focus of 0 μm, dose step of 1 mJ/cm^2 and focus step of 0.04 μm. A total of 11 steps in dose and 9 steps in focus were used.

The metrology was done on a Hitachi CG4000 CD SEM using Design Gauge. Within each acquired image, the CD has been averaged over as many features as possible, up to 25 times. All the features have been measured along both x and y directions, and each feature has been averaged over 25 dies across the wafer in order to ensure statistical quality. An ellipse measurement algorithm has been used for all the features except for elongated CH in y direction in the sub-module CH 3, which had to be measured using a gap measurement algorithm, as the ellipse fit would inaccurately measure the elongated portion of the CH. However, the two algorithms are not similar in term of repeatability. In fact, the error on the average CD calculated across the wafer was found to be 0.5 nm or lower for all features except the elongated CH in y direction, a consequence of the local nature of the gap measurement algorithm, as shown in Figure 5.

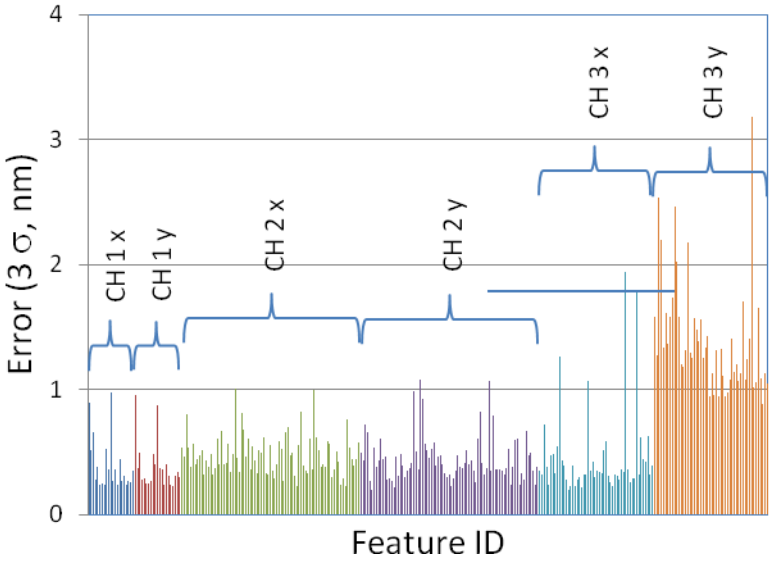

Figure 5: Experimental error for the investigated features.

5. EUV MODEL CALIBRATION

The EUV model calibration approach used is the joint optimization of an optical model and a resist model. The optical model is based on NXE:3100 with a NA of 0.25 and a σ of 0.81. The Tachyon NXE integrated conventional pupil is used, which is a Zeiss design target of the standard NXE:3100 conventional pupil. The resist model is a Tachyon FEM+ resist model that consists of different Gaussian diffusion image terms [7]. The Gaussian sigmas were optimized during regression. Flare is simulated using the flare map generated from mask pattern density and the point spread function (PSF) provided by Zeiss for IMEC's NXE:3100 scanner. Inter field effects and exit aperture effects were considered during flare map generation [8]. Figure 1 shows an overview of the flare map. The maximum flare level in the layout is about 5.6%. The flare level change through scan direction corresponds well with the design dummy density variation. The flare drops slightly close to the edge of the field and the signature high stray light from border effects does not occur in this case because there is a 1 mm space between neighboring exposure fields. Shadowing effects were simulated by using a calibrated slit center HV bias to calculate each edge's bias based on the slit location of the edge. The fitting

showed that an HV bias per edge of 1.5 nm was optimal in the center of the slit, and the correction is implemented through slit by using an analytical formulation of the expected behavior.

The model calibration used the sub-module CH 1, CH 2 and CH 3 in the center of the mask (0,0), as well as the sub-module CH 1 in top scan in the center of the slit (0,+2). The cost function of the calibration is the weighted RMS of the gauge model error. The gauges were not weighted equally during calibration. CH 3 gauges were weighed lower (0.5 and 0.1 for x and y, respectively) because the metrology method used was different from the other gauges. Scan top CH 1 was also weighted lower (0.2) because some through scan artifacts were identified. More details will be discussed later in this paper.

The calibration achieved model error RMS of 1.072 nm for all the 350 gauges. Here model error is defined as (model CD – wafer CD). Figure 6 shows an overview of the calibration result. Figure 6a is the RMS of each group of patterns and Figure 6b gives the mean model error and error range of each group. All CH 1 at scan center and CH 2 have a small RMS and range. CH 1 at scan top shows worse fitting and the mean error is biased to the positive side. CH 3, especially on y (long) direction, has the worst fitting among all groups as expected. As discussed, CH 3 y was measured using a different measurement method from the other groups, so a systematic deviation can exist. CH 3 x, although used the same elliptical fitting method as other groups, suffers from a measurement accuracy issue because the elliptical fitting is not suitable for relatively long bars, as discussed above.

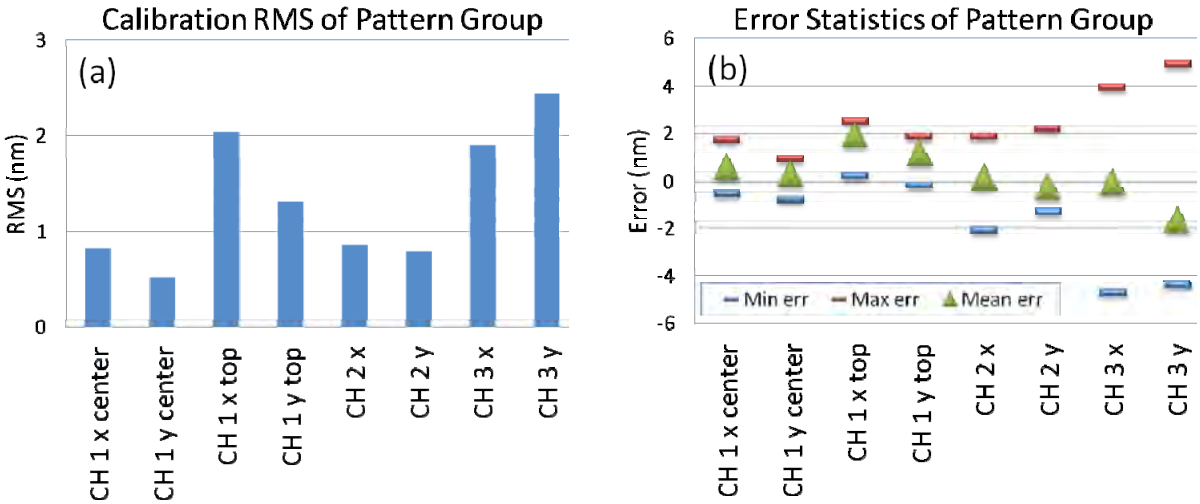

Figure 6: Overview of the model fitting results: (a) RMS error between measured CD values and modeled CD values for each pattern group; (b) Minimum, maximum, and mean fitting error between measured and modeled CD.

Looking at the symmetric contact array (CH 1), we noticed the CD difference between x and y direction is relatively small compared to the 1.5 nm per edge optimized from calibration. This is due to the strong optical interaction between contact edges. This interaction would be stronger with smaller contact size, and thus causes more similar x and y printing. The model prediction and part of the wafer data on Figure 7a agree with this. However, we remark that the y CD on wafer becomes even larger than the x CD when contact size is smaller than 34 nm, which is somewhat counterintuitive. In order to try to explain the effect, a calibration with the design aberrations of IMEC's NXE:3100 provided by Zeiss was performed, but the result still could not explain this behavior (Figure 7b).

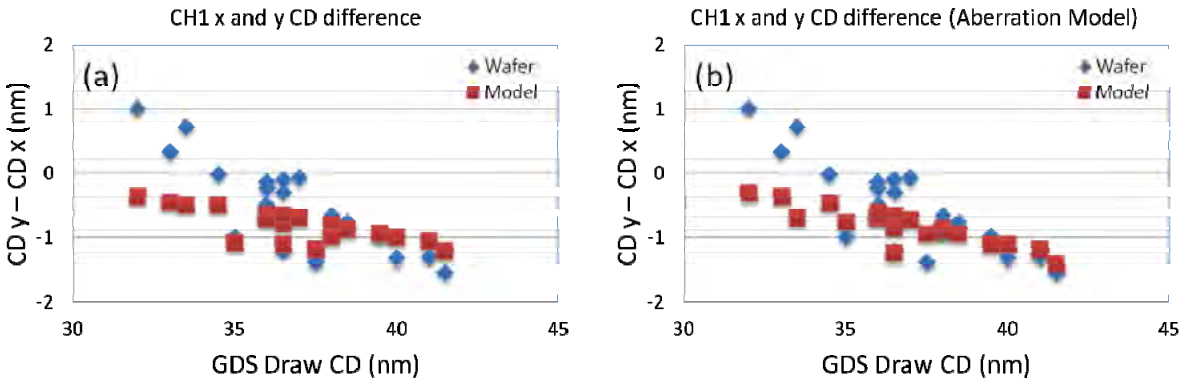

Figure 7: CH 1 x and y CD difference. (a) No aberration used in model. (b) Aberration used in model.

6. EUV MODEL VALIDATION

To validate the model prediction accuracy, we collected a large set of wafer CD data, as discussed above. Most of the validation data were collected from the second uniform wafer exposed. Through slit prediction also gives a small RMS of 0.78 nm. Almost all gauges have model error within +/-2 nm (Figure 8). There are two points with model error of ~3 nm, which are located at the very edge of the slit.

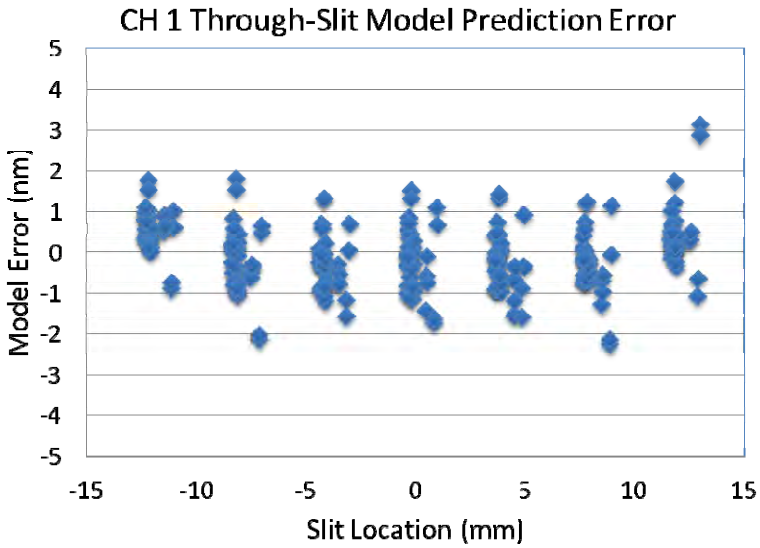

Figure 8: Model Error of CH 1 through slit.

CH 1 through scan data were actually collected on both first and second wafer in order to confirm the observed variation through scan. Unfortunately, the field top measurements of wafer 2 were lost during measurement. Figure 9 shows the through scan model CD error of wafer 1 and wafer 2. The GDS Y coordinate 0 corresponds to field bottom edge, and 33 corresponds to field top edge. We can see that, for both wafers, the model matches wafer well at scan direction center, but predicts CD larger than measured on wafer towards top and bottom ends of the scan direction. The RMS measured for the first and second wafer was1.46 nm and 1.11 nm, respectively.

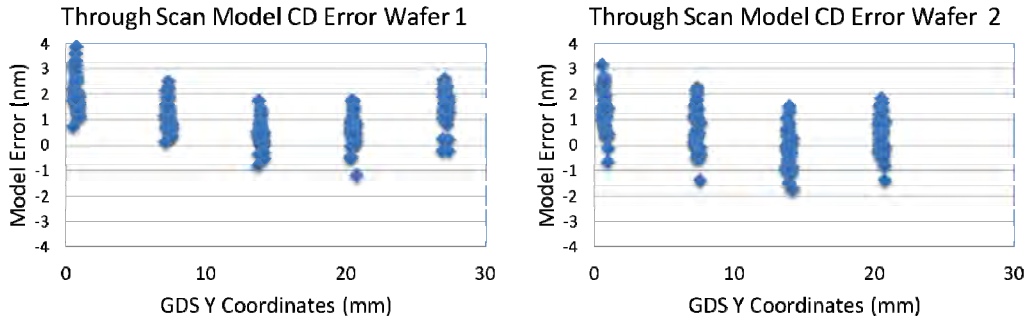

Figure 9: Model error of CH 1 through scan direction for both wafers.

Additional investigation indicated that wafer CD and model CD have different through scan trend signature. Figure 10 shows such trends for three patterns. Wafer CD is maximum at field center and decreases toward field top and bottom, while model CD is almost monotonically decreasing from field bottom to field top as a consequence of the flare variation caused by the different tiling density.

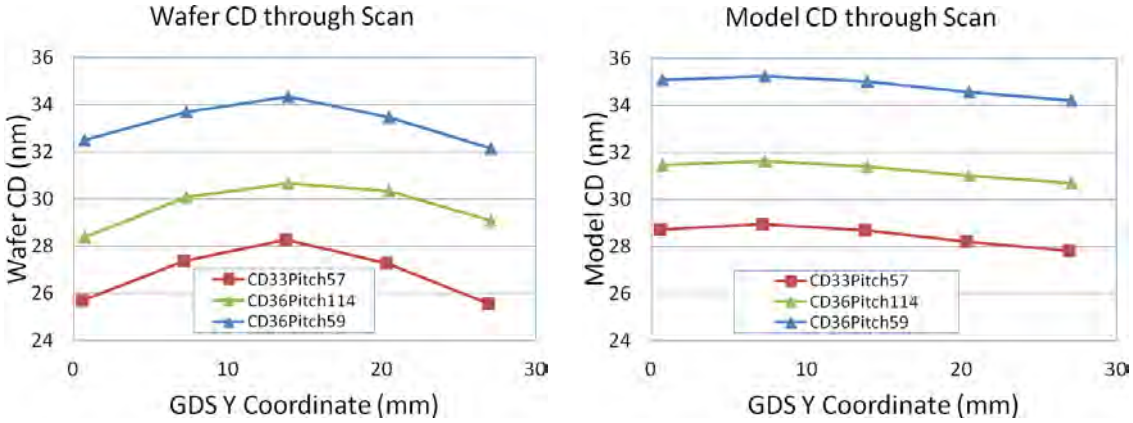

Figure 10: Through scan wafer CD (left) and model CD (right). The model CD trend matches with the flare level design of the mask.

The wafer CD trends observed in Figure 10 correlate extremely well with the radial signature of the mask, as shown in Figure 11, where the average wafer CD of the module CH 1 is plotted for wafer 1 and compared to the trend of the mask CD along y for 32 nm dense CH. These results indicate that even though the quality of the mask was quite good, the mask CD signature of 1.31nm is large enough to dominate the effect of flare at wafer level, where a signature of 1.89nm was found for wafer 1.

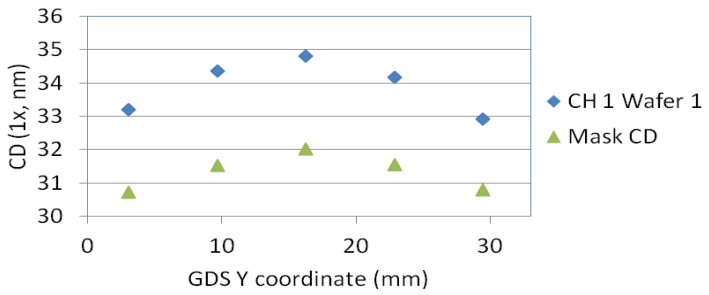

Figure 11: Through scan mask CD and wafer CD. The mask CD trend matches well with the observed wafer CD trend.

Finally, the SEM pictures for the sub-module CH 4 are compared with the model predicted contours in Figure 12, showing a nice agreement between simulation and experiment. All the contours were obtained without altering any of the model settings. In Figure 12 a, we compared the model prediction with the wafer results for the sub-module CH 3 for elongated CH, where the CH metrology had both accuracy and precision issue. Also in this case, the simulation is able to neatly match the wafer data, further strengthening the confidence in the modeling.

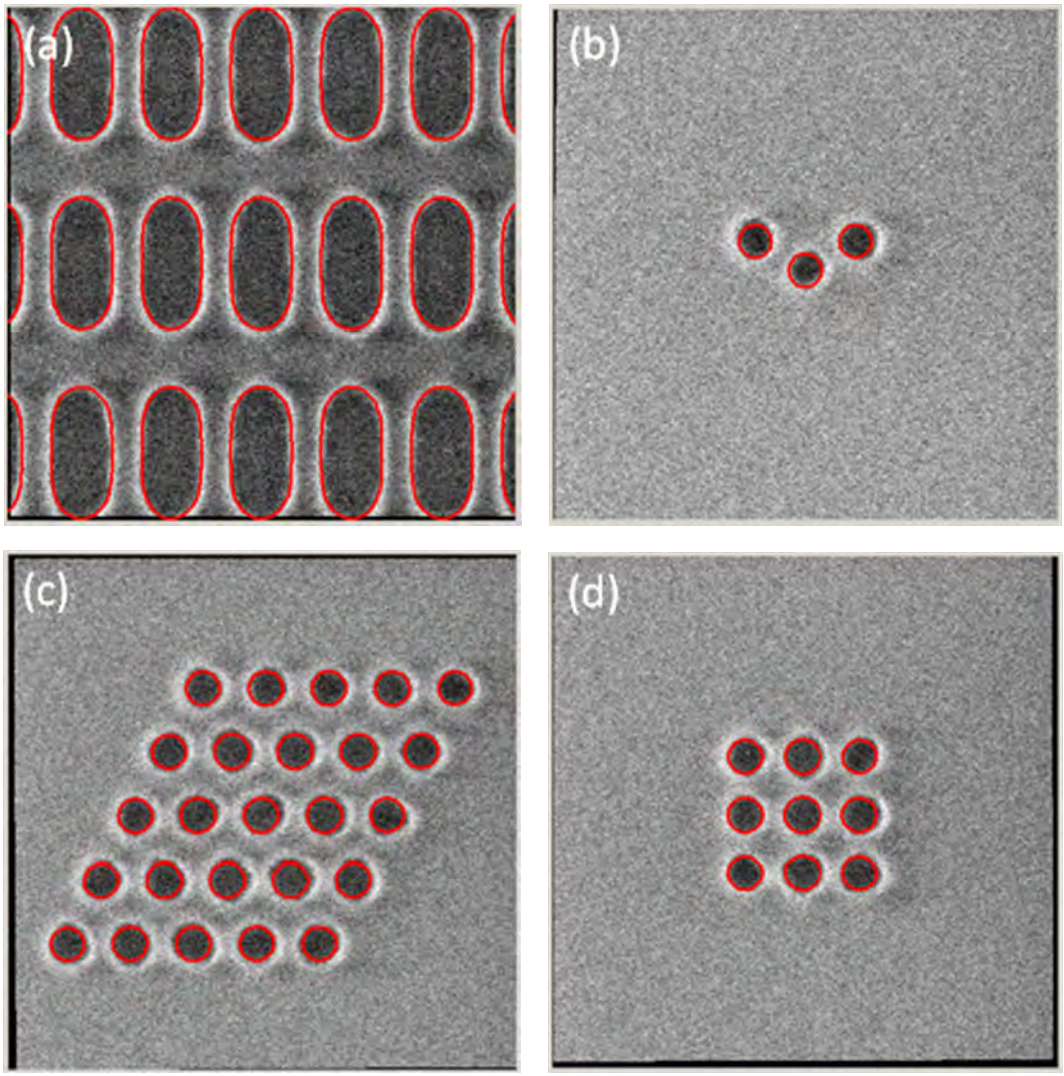

Figure 12: Selected model contours and SEM wafer images for the sub-module CH 3 (a) and CH 4 (b, c, and d). The contours nicely match the wafer data

7. OPC ACCURACY

In Figure 13 the uncorrected and corrected proximity curves for 27 nm dense CH are compared to the modeling predictions, accounting as well for the mask proximity signature in Figure 3. As expected, the model can reproduce well the proximity signature through pitch. In addition, the proximity signature is flattened by using the predicted bias at mask. The noise in both the experimental and simulated results in the case of the corrected curves is caused by the limitation imposed by the available step size at mask (0.5 nm) intrinsically limiting the quality of the implementable correction.

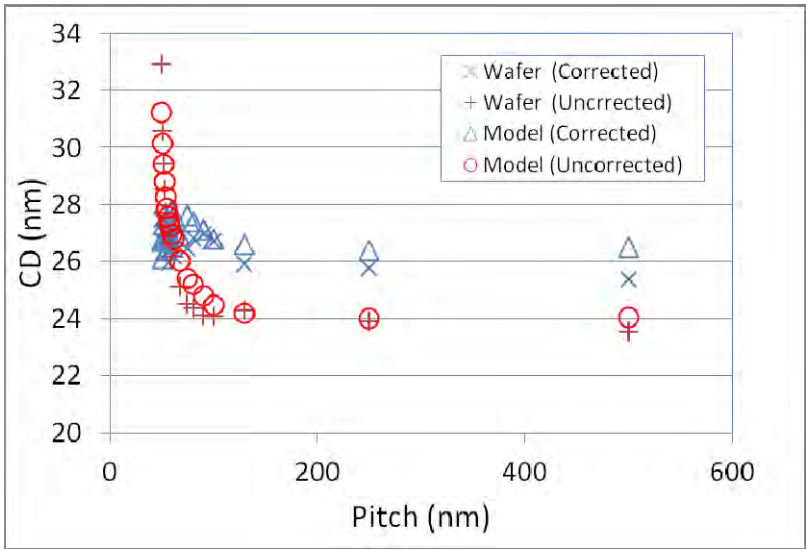

Figure 13: Measured and modeled 27 nm CH proximity curves with and without correction.

8. CONCLUSIONS

A model calibration exercise for 2D structures has been performed on a pre-production EUVL scanner (ASML NXE:3100) using Brion's Tachyon NXE EUV system. A purposely produced EUV mask has been used in the exercise, and extensive metrology qualification of the reticle has been performed in order to discriminate between modeling, scanner and mask effects. The mask demonstrated good MTT (~ -1 nm), good CDU (~ 1.8 nm) and limited proximity (iso-dense bias ~1.2 nm), together with a radial CD signature. The model calibration exercise yielded a low RMS = 1.072. Similarly, the verification through slit and through scan yielded RMS values close to 1. The results indicate that the radial mask signature is indeed dominant on the wafer data, thus masking the mild impact of flare expected for such a dark field layout. The shadowing compensation is observed to be effective, although a shadowing reversal is observed for the smallest CD. Simulations accounting for the optical aberration were performed, but they were unable to explain the observed effect. The quality of the OPC correction was also tested by compensating the proximity curve of 27 nm CH through pitch, and the results strengthen the confidence in the model.

9. ACKNOWLEDGEMENT

We wish to thank the ASML on site team as well as the one in Veldhoven for their support. We are indebted with the Hitachi on site team for their continuous help. We wish to thank Jan Hermans for supporting the exposures and Vicky Philipsen and Keith Gronlund for many fruitful discussions.

REFERENCES

[1] Veloso, A., *et al.*, "Full-field EUV and immersion lithography integration in 0.186μm2 FinFET 6T-SRAM cell", Proc. IEDM, 1 (2008).
[2] Veloso, A., *et al.*, "Demonstration of scaled 0.099μm2 FinFET 6T-SRAM cell using full-field EUV lithography for (Sub-)22nm node single-patterning technology" Proc. IEDM, 1 (2009).
[3] Lorusso, G., F., Goethals, A., M., Jonckheere, R., Hermans, J., Ronse, K., Myers, A., M., Kim, I., Niroomand, A., Iwamoto, F., and Ritter, D., "Extreme ultraviolet lithography at IMEC: Shadowing compensation and flare mitigation strategy", J. Vac. Sci. Technol. B Volume 25, Issue 6, pp. 2127-2131 (2007).
[4] Lorusso, G., F., Van Roey, F., Hendrickx, E., Fenger, G., L., Lam, M., Zuniga, C., Habib, M., Diab, and H., Word, J., "Flare in extreme ultraviolet lithography: metrology, out-of-band radiation, fractal point spread function, and flare map calibration", Journal of Micro/Nanolithography, MEMS, and MOEMS, 8, 4, (2009).
[5] Fenger, G., L., Lorusso, G., F., Hendrickx, E, and A. Niroomand, "Design correction in extreme ultraviolet lithography", J. Micro/Nanolith. MEMS MOEMS 9, 043001 (2010)

[6] Abdo, A., Viswanathan, R., “The feasibility of using image parameters for test pattern selection during OPC model calibration” Proc. SPIE 7640, 76401E (2010).
[7] Cao, Y., Lu, Y.-W., Chen, L., and Ye, J., "Optimized hardware and software for fast full-chip simulation" Proc. SPIE 5754, 407 (2005).
[8] Driessen, F., A., J., M., Davydova, N. Jiang, J., Kang, H., Vaenkatesan, V., Oorschot, D., Kim, I., S., Kang, S., N., Lee, Y., Yeo, J., Gronlund, K., Liu, H., Y., van Ingen-Schenau, K., Peeters, R., Wagner, C., Zimmermann, J., and Schumann, O., “Holistic lithography for EUV: NXE:3100 characterization of first printed wafers using an advanced scanner model and scatterometry” Proc. SPIE 8166, 81660Z (2011).